A comparison of numerically and experimentally obtained in-plane responses of a full-scale unreinforced masonry building frame

A. Pir, L.S. Hogan, D.Y. Dizhur, K.Q. Walsh, & J.M. Ingham

Department of Civil and Environmental Engineering, University of Auckland, New Zealand.

ABSTRACT: Pushover analysis is a popular technique to determine the displacement capacity and failure mechanisms of assemblies of building components or global building behaviour. As pushover analysis is often used for the assessment of unreinforced masonry (URM) buildings, there is a need to benchmark existing modelling frameworks against large scale testing in order to assist in the development of best practice guidelines. Hence, a study was performed to assess the suitability of existing pushover analysis techniques to represent the in-plane response of a clay brick URM building frame. Utilising material and geometrical properties determined from in-situ measurements and laboratory testing, a "blind" pushover analysis of a three-storey frame from an early 1900s URM building located in central Auckland, New Zealand was performed using the *SAP2000*^{TM} (2011) software package and following national and international assessment guidelines. The results obtained from the simulated pushover analysis were compared to those obtained from experimental in-situ pushover testing of the building frame, and recommendations regarding the in-plane pushover analysis of URM frames were made based on the results.

Keywords: pushover analysis, URM, rocking wall, seismic response, clay brick, earthquakes, heritage buildings

1 INTRODUCTION

Pushover analysis is a nonlinear assessment method used to evaluate the predicted response of buildings and building components when subjected to lateral earthquake loading. The method is based on nonlinear force-deformation relationships of substructures and can be used to assess building strength capacity and post-yielding behaviours. The brittleness of the masonry material potentially results in the formation of nonlinear behaviour at low displacement demands. An equivalent frame approach for assessing unreinforced masonry (URM) piers and spandrels was introduced by Dolce (1989) which was adopted by Knox (2012) and Sarkar et al. (2015). This approach is widely utilised by practicing engineers in place of costly finite element methods using shell and solid elements.

The case study building modelled in this research programme was an early 1900s URM building experimentally tested for in-plane response. The west wall of the building was subjected to quasi-static and impulse loads at the roof level, and the tested URM wall was pushed to the initiation of cracking and rocking in the URM piers. More information on the building and experimental studies are presented in Hogan et al. (2015a, 2015b). As reported herein, a blind pushover numerical simulation was carried out to predict the lateral response of the URM wall, and the predictions were compared to the experimental results. The URM wall in-plane assessment methods as presented in NZSEE (2015) and ASCE 41-13 (2014) include linear and nonlinear analytical guidelines used to predict the seismic performance of URM walls in-plane.

2 ANALYTICAL MODEL AND VALIDATION

2.1 URM equivalent frame

Based on the Dolce (1989) equivalent frame model, a URM wall loaded in-plane can be discretised into frame elements (i.e. piers, spandrels, and rigid connection zones). The effective heights of the URM piers based on the proposed criteria of the Dolce (1989) method are shown in Figure 1. Knox (2012) carried out experimental and numerical research on URM walls and employed the equivalent frame concept to predict the nonlinear in-plane response of laboratory-built URM walls. According to Knox (2012), the numerical modelling of URM walls using the equivalent frame approach was found to be generally compatible with experimental results.

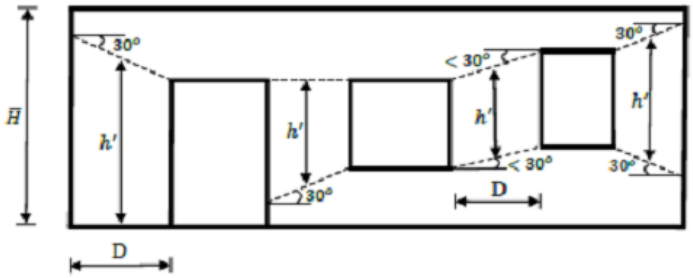

Figure 1. Piers effective heights as proposed by Dolce (1989)

In the considered wall of the subject building, a reinforced concrete (RC) bond beam existed at each floor level. Hence, the spandrel beams at the first and second levels of the equivalent frame model were modelled as composite elements (i.e., URM and RC). The schematic drawings of the tested URM wall and its equivalent frame are illustrated in Figure 2.

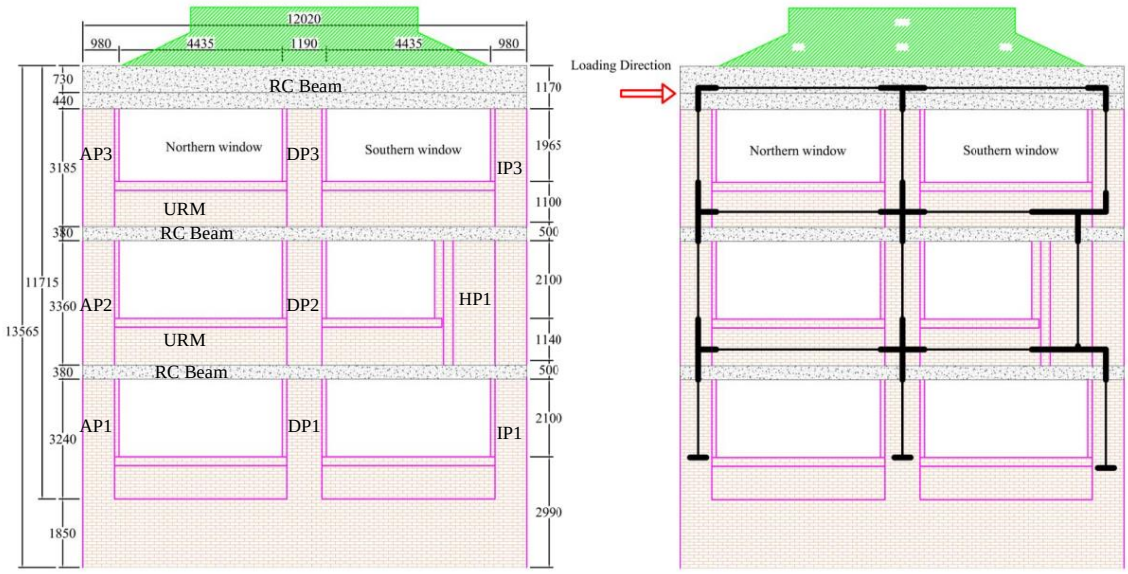

a) Components of the tested wall b) Equivalent frame of the tested wall

Figure 2. Schematic drawings of the tested wall

2.2 Material properties

In the study reported herein, material properties were experimentally determined and subsequently employed in the model of the case study building in order to accurately simulate the nonlinear behaviour of each component. The experimentally measured mechanical characteristics of the masonry prisms included the mean compressive strength (f'_m), modulus of elasticity (E_m), and the

mean masonry bed joint shear strength f'_{jv} which were equal to 6.3 MPa, 5632 MPa, and 0.44 MPa respectively. The mean compressive strength and Young's modulus of URM prisms were obtained using the procedures reported in ASTM C1314 (2011) which represents the un-crack characteristics of URM material. The horizontal compressive strength (f'_{mh}) and the shear modulus of masonry material (G_m) were assumed equal to $0.5f'_m$ and $0.4f'_m$ respectively, in accordance with NZSEE (2015) and ASCE 41-13 (2014) guidelines. The mean measured concrete compressive strength and modulus of elasticity were 18.5 MPa and 18,190 MPa, respectively.

2.3 **Strength-deformation relation of URM components**

2.3.1 *URM pier in-plane capacity*

URM pier failure is potentially governed by four fundamental mechanisms. According to NZSEE (2015), the lateral load capacity corresponding to each of the four mechanisms can be calculated by the following formulae:

$$V_r = \frac{0.9(\alpha P + 0.5P_W)L_w}{H_{eff}} \quad (1)$$

$$V_{tc} = \frac{(\alpha P + 0.5P_W)L_w}{h_{eff}}\left(1 - \frac{f_a}{0.7f'_m}\right) \quad (2)$$

$$V_{dt} = f_{dt}\, A_n \beta \sqrt{\left(1 + \frac{f_a}{f_{dt}}\right)} \quad (3)$$

$$V_s = 0.7(A_n c + \mu_s (P + P_W)) \quad (4)$$

Where V_r, V_{tc}, V_{dt}, and V_s are the maximum predicted capacities for rocking, toe crushing, diagonal tensile cracking, and bed joint sliding failure mechanisms, respectively. In these formulae, P and P_w represent the overburden load applied at the top of the effective height of the pier plus the pier self weight. L_w and h_{eff} represent the length and effective height, respectively, of the pier, and f_a and f'_m represent the axial stress at the bottom of pier and masonry prism compressive strength, respectively. The masonry diagonal tensile stress and net area are denoted by f_{dt} and A_n, and parameters "c" and "μ" represent masonry cohesion and friction respectively.

The maximum capacity of each pier is governed by the minimum of the calculated in-plane strengths of the four failure mechanisms. When discounting the presence of flanges, the predicted shear strengths for each pier of the case study wall are listed in Table 1 with the minimum capacity included in bold, indicating that the dominant failure mode for all piers was predicted to be rocking. The generalised strength-deformation diagram for the rocking mechanism as prescribed by NZSEE (2015) and ASCE 41-13 (2014) is shown in Figure 3.

Table 1. Predicted pier capacity

Pier ID*	Axial Load (kN)**	V_r (kN)	V_{tc} (kN)	V_{dt} (kN)	V_s (kN)	Axial Load (kN)***	$V_{r,flanged}$ (kN)
AP1	131	**33**	34	164	195	156	**42**
AP2	79	**21**	23	129	174	93	**28**
AP3	33	**10**	11	80	121	36	**15**
DP1	240	**66**	68	194	264	236	**72**
DP2	156	**45**	47	157	229	153	**49**
DP3	87	**29**	31	125	199	85	**31**
HP1	87	**42**	45	205	297	104	**49**
IP1	150	**30**	30	177	204	183	**38**
IP3	33	**9**	10	81	122	36	**11**

* Pier IDs are illustrated in Figure 2-(a)
** Axial load at the top of the simplified piers
***Axial load at the top of the flanged piers

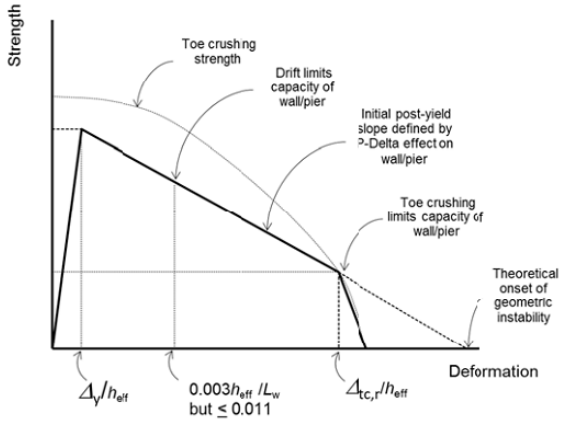

Figure 3. Generalised strength-deformation relation for URM piers (NZSEE 2015)

The displacement corresponding to maximum rocking strength is symbolised by Δ_y. The toe crushing limit capacity and its corresponding deformation, $\Delta_{tc,r}$, were defined by utilising the moment-curvature approach prescribed by NZSEE (2015). The toe crushing deformation limit can be determined from the following formula (Moon 2004):

$$\Delta_{tc,r}=h_{eff}^2\frac{(0.8)(0.0035)}{\left(\frac{P_b}{0.8f'_m b_w}\right)}\left(\frac{1}{3}\right) \quad (5)$$

Where P_b represents the axial load at the bottom of the pier, b_w is the pier width, and the other parameters are as defined previously.

2.3.2 *Effect of flanges on the URM pier rocking capacity*

According to NZSEE (2015), the in-plane response of URM piers is significantly influenced by the presence of flanges. Yi et al. (2008) developed a set of formulae to predict the capacity of flanged walls based on internal stress distribution in the URM walls. In the current study, the primary shear capacities of the piers were calculated according to NZSEE (2015) while neglecting the flanges, and the effects of flanges on rocking capacity (the assumed dominant mechanism) were evaluated by considering the flange self-weight acting on the flange geometrical centroid, with updated values for rocking capacity provided in the far right columns of Table 1. The pier details are illustrated in Figure 4.

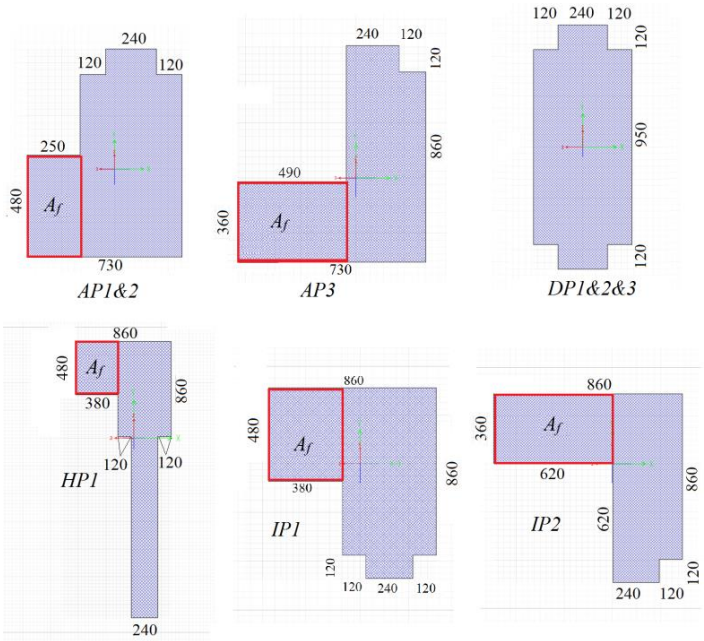

Figure 4. Pier cross-sections (The flange area is indicated by A_f)

2.3.3 *Spandrel flexural and shear capacity*

The URM and RC spandrel compressive models were based on the "Park-Kent model" (Kaushik et al. 2007), and it was assumed that the URM material behaved as weak concrete (compared to the concrete compressive strength of RC beams) with a mean compressive strength of 6.3 MPa. Each spandrel was modelled as a composite component by using asymmetrical moment-rotation relationships based on flexural equilibrium as shown in Figure 5. The shear capacity of the URM spandrel material was calculated according to NZSEE (2015). Compared to the shear strength of the RC beam, the URM spandrel shear strength was relatively insignificant. Hence, the shear capacity of the RC beam by itself was assumed to represent the spandrel shear strength.

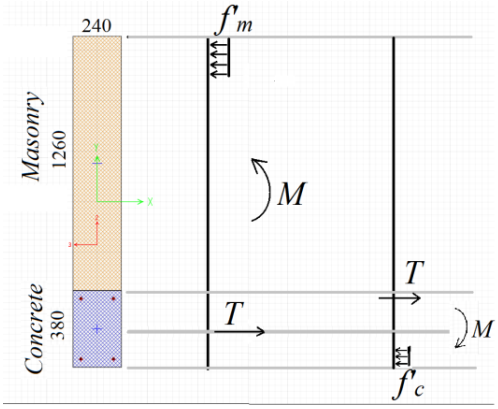

Figure 5. Schematic of the flexural equilibrium of a composite spandrel for positive and negative flexure

2.4 **Numerical modelling**

SAP2000^{TM} was employed as the platform for predicting the nonlinear response of the case study URM building wall. *SAP2000*^{TM} allows the user to define the shear and flexural hinge properties for asymmetrical and composite sections. Equivalent frame components were defined according to the measured geometries of the in situ building wall. To assess the in-plane shear capacity of the tested URM wall, two sets of pier cross-sections, the simplified and as-built flanged piers, were defined by using the "section designer" in *SAP2000*^{TM}. The first pier set included simplified pier sections for which the effects of the flanges on the URM wall were neglected. The second pier set consisted of modelled piers with as-built cross-sections. The strength-deformation relationship for each URM pier was defined by assigning a nonlinear shear hinge at midheight based on NZSEE (2015) and ASCE 41-13 (2014) recommendations. The shear hinge was the preferred simulation option for modelling of the rocking mechanism (the dominant mechanism) since the shear strength corresponding to the relative displacement of piers could be modelled directly in accordance with NZSEE guideline (shown in Figure 3). In order to calibrate the shear hinge responses to lateral deformation, each pier was initially subjected to an isolated pushover analysis. The spandrels were modelled according to measured geometries with three plastic hinges assigned to represent the flexural and shear behaviour of the composite RC beam. Flexural plastic hinges were assigned to each end of every spandrel, and shear hinges were assigned to the midlength of every spandrel. The connections between piers and spandrels were modelled as rigid zones by considering offset lengths at the ends of each element based on the recommendations of Dolce (1989).

3 **IN-PLANE PUSHOVER PREDICTED RESPONSE**

To compare the numerical pushover curves with the experimental results, a single point load was applied at the roof level in place of typical pushover load distribution which is a linearly increasing load at each floor. The base shear force corresponding to the roof displacement was recorded in 1000 analytical steps by imposing an incremental displacement at the roof level of the wall up to 0.4 mm in each step. With increasing lateral deformation, rocking mechanisms formed at the top piers, at the shear hinges which were defined in order to simulate a rocking mechanism, also developed at the top piers after an insignificant deformation of 1.5 mm. Subsequently, the shear capacity degraded due to toe crushing mechanism in piers AP3, DP3, and IP3. The final collapse stage of the modelled URM

wall as shown in Figure 6 was governed by toe crushing in the top floor piers. The maximum shear capacities of the simulated wall were predicted to occur at 1.75 mm and 2 mm of roof level displacement in the simplified and flanged models, respectively.

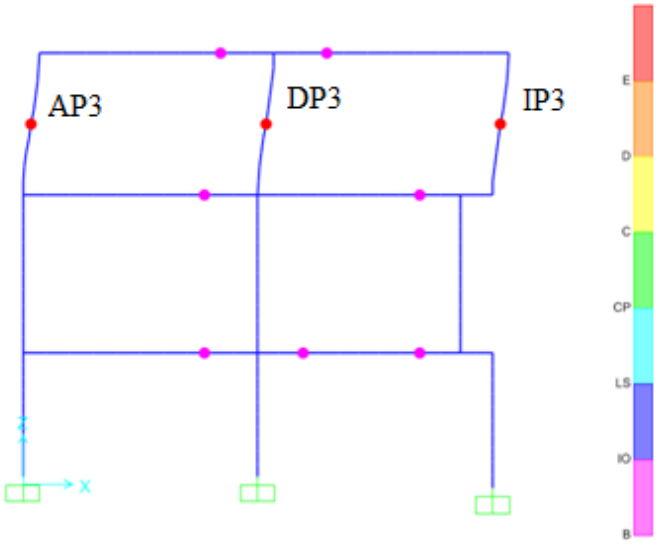

Figure 6. Deformed equivalent frame

The simulated pushover capacity curves for the URM wall models with the simplified and flanged cross-section configurations, respectively, are illustrated in Figure 7. Each drop in the numerical pushover curve represents the complete loss of lateral load carrying capacity of a pier at the roof level which was defined according to the pier deformation limits as shown in Figure 3. The model with as-built flanged piers resulted in an 18% increase in predicted maximum lateral capacity compared to the simplified model, due to predicted increases in the rocking capacity and toe crushing strength. The predicted pushover curve of the modelled wall with flanged piers had a lower lateral drift capacity compared to the simplified model due to differences in the toe crushing limit capacity, consistent with the results reported by Yi et al. (2008), explaining the earlier lateral strength loss of the IP3 pier in the flanged model. At the roof level, the IP3 pier was the sole pier with a flange located at the toe. Furthermore, the deformation capacity corresponding to toe crushing would be reduced by any increase in the axial load (Equation 5).

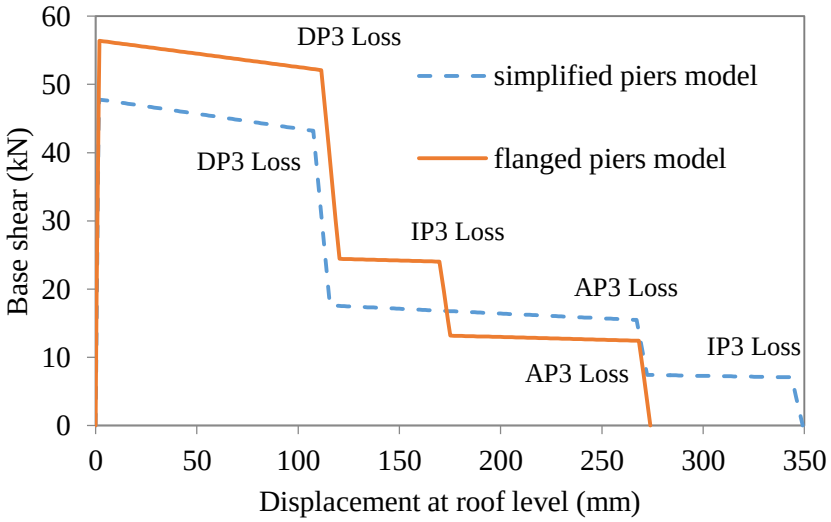

Figure 7.Base shear-displacement curves of the tested wall

4 COMPARISON OF PREDICTEDAND EXPERIMENTAL RESULTS

The URM wall shown in Figure 8 (as modelled in Figure 2) was subjected to in-situ quasi-static and impulse loading, and the load-deformation measurements were recorded over eight loading cycles. Due to limitations in the loading capacity of the test equipment relative to the measured strength of the wall, the building wall was likely not loaded to its ultimate strength. The maximum applied load to the in situ wall was measured as 55 kN (Figure 9).

Figure 8. The URM wall subjected to in-plane load

Comparison between numerical and experimentally measured pushover results (Figure 9-a) indicated that the simplified numerical model underestimated the minimum possible strength of the tested wall and the flanged model predicted the pier strength closer to the minimum possible strength of the tested wall. The displacements corresponding to the maximum numerically measured shear strength, 55 kN, were 1.9 mm for the flanged pier model and 3.75 mm for the experimental results, respectively (Figure 9-b). The initial stiffnesses of the tested and the simulated walls were approximately identical, and the difference between the in-plane stiffness of the experimentally tested wall and simulated wall could be explained by the rocking mechanism of a pier which is simulated as rigid-body rotation and independent from the member stiffness in the model. In the experimental study, approximately, 46% of the total 0.3 mm deformation at the middle pier was due to rocking (Hogan et al. 2015b) which could explain the 51% difference in the simulated and experimentally measured displacements corresponding to 55 kN. The initial and secant stiffnesses referred to the base shear-deformation ratios corresponding to the initial linear and the maximum experimentally measured shear strength, respectively.

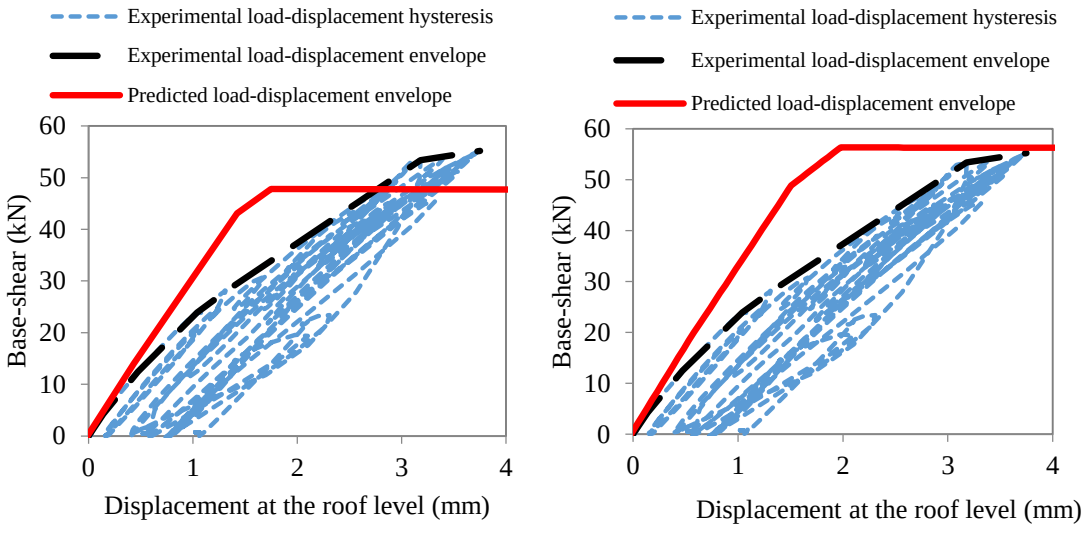

a) Simplified piers

b) Flanged piers

Figure 9. Load-displacement curves

5 CONCLUSION

An analytical model for the in-plane assessment of a case study URM wall was presented based on an equivalent frame approach as well as NZSEE (2015) and ASCE 41-13 (2014) guideline recommendations. The maximum in-plane load capacity of the URM wall was predicted by performing a blind pushover analysis. The maximum predicted in-plane shear capacities corresponding to the simplified and flanged pier cross-sections were 47 and 56 kN respectively, which indicated that by taking the flanges into account, an 18% increase in the shear capacity of the case study URM wall was predicted. Hence, it was concluded that considering the flanged cross-section in the pushover model would likely result in more realistic in-plane strengths. Compared to the experimentally measured pushover result, the predictive model underestimated the actual in-plane wall capacity. Compared to the tested wall, the initial stiffness of the simulated wall was 6% higher. Furthermore, the higher measured displacements of the tested wall at the roof level corresponding to 55 kN demonstrated that the numerical model overestimated the secant wall stiffness by 51%.

6 REFERENCES:

ASCE/SEI 41-13. 2014. Seismic evaluation and retrofit of existing buildings. American Society of Civil Engineers, Washington D.C, United States.

ASTM C1314. 2011. Standard test method for compressive strength of masonry prisms. American Society for Testing and Materials, Pennsylvania, United States.

Dolce M. 1989. Models for in-plane loading of masonry walls. Corso sul consolidamento degli edifici in muratura in zona sismica. Ordine degli Ingegneri,Potenza. (Italian)

Hogan L.S., Walsh K.Q., Beskhyroun S., Ingham J.M., and Dizhur D.Y. 2015a. Contribution of timber-framed partition walls to the dynamic characteristics of an unreinforced masonry building. New Zealand Society of Earthquake Engineering Technical Conference. *10-12 April 2015*. Wellington.

Hogan L.S., Walsh K.Q., Ingham J.M., and Dizhur D.Y. 2015b. Experimental pushover testing of a full-scale existing unreinforced clay brick masonry building. 10th Pacific Conference on Earthquake Engineering. *6-8 November 2015*. Sydney, Australia.

Knox L.C. 2012. Assessment of perforated unreinforced masonry walls responding in-plane. University of Auckland. PhD Thesis. Auckland.

Kaushik H.B., Rai D.C., and Jain S.K. 2007. Stress-strain characteristics of clay brick masonry under uniaxial compression. Journal of Materials in Civil Engineering, 19(9).728-738.

Moon F.L. 2004. Seismic strengthening of low-rise unreinforced masonry structures with flexible diaphragms. Georgia Institute of Technology. PhD Thesis. Georgia.

NZSEE 2015. Assessment and improvement of the structural performance of buildings and earthquakes - recommendations of a NZSEE study group on earthquake risk buildings. New Zealand Society for Earthquake Engineering. Wellington.

Sarkar A., Halder L., and Sharma R. 2015. Seismic damage evaluation of unreinforced masonry buildings in high seismic zone using the nonlinear static method. Advances in Structural Engineering.1039-1053. Springer India.

SAP2000 Ultimate. 2011. Structural analysis program. V-15.1. Computers and Structures Inc, Berkeley, CA, USA.

Yi T., Moon F.L., Leon R.T., and Kahn L.F. 2008. Flange effects on the nonlinear behaviour of URM piers. The Masonry Society Journal. 26(2).31-42.